ACS NANO

www.acsnano.org

ARTICLE

Single-Particle Measurements Reveal the Origin of Low Solar-to-Hydrogen Efficiency of Rh-Doped $SrTiO_3$ Photocatalysts

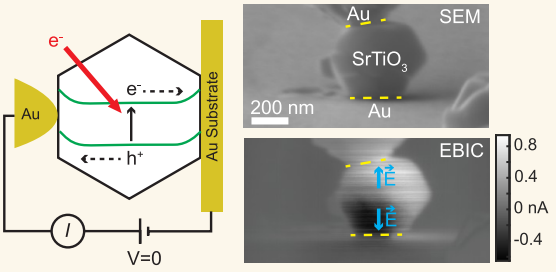
Brian Zutter, Zejie Chen, Luisa Barrera, William Gaieck, Aliya S. Lapp, Kenta Watanabe, Akihiko Kudo, Daniel V. Esposito, Rohini Bala Chandran, Shane Ardo, and A. Alec Talin*

Cite This: *ACS Nano* 2023, 17, 9405−9414

Read Online

ACCESS | Metrics & More | Article Recommendations | Supporting Information

ABSTRACT: **Solar-powered photochemical water splitting using suspensions of photocatalyst nanoparticles is an attractive route for economical production of green hydrogen. $SrTiO_3$-based photocatalysts have been intensely investigated due to their stability and recently demonstrated near-100% external quantum yield (EQY) for water splitting using wavelengths below 360 nm. To extend the optical absorption into the visible, $SrTiO_3$ nanoparticles have been doped with various transition metals. Here we demonstrate that doping $SrTiO_3$ nanoparticles with 1% Rh introduces midgap acceptor states which reduce the free electron concentration by 5 orders of magnitude, dramatically reducing built-in potentials which could otherwise separate electron−hole (e−h) pairs. Rhodium states also function as recombination centers, reducing the photocarrier lifetime by nearly 2 orders of magnitude and the maximum achievable EQY to 10%. Furthermore, the absence of built-in electric fields within Rh-doped $SrTiO_3$ nanoparticles suggests that modest e−h separation can be achieved by exploiting a difference in mobility between electrons and holes.**



KEYWORDS: *photoelectrochemical water splitting, strontium titanate, semiconductor nanoparticle, semiconductor heterojunction, transition metal doping*

INTRODUCTION

Solar-driven water splitting is an attractive route to generate green hydrogen, an easily storable and clean fuel. Of the possible schemes currently investigated, approaches based on nanoparticle photocatalyst suspensions are projected to be among the most cost−effective.[1−5] However, these projections are based on a >10% solar-to-hydrogen (STH) conversion efficiency, while current state-of-the-art STH efficiencies do not exceed[6] ∼5% and all large-scale demonstrations are below[7] 1%. Thus, a dramatic improvement in STH efficiency is needed to realize a practical photocatalytic (PC) system for solar water splitting.

The PC water splitting process (Figure 1a) comprises three basic steps: (1) light absorption, (2) transport of photocarriers to the surface of the nanoparticle, and (3) hydrogen or oxygen evolution (often aided with a cocatalyst). Optimizing all three steps within a single material system is a considerable challenge. To date, $SrTiO_3$ nanoparticles are among the most promising due to their high stability[8] and demonstrated ability to perform unassisted solar water splitting.[9−11] However, with a bandgap of 3.2 eV, unintentionally doped $SrTiO_3$ only absorbs a small fraction of the solar spectrum. To increase visible absorption, dopants like N, C, S and various transition metals have been introduced with the goal of forming a midgap impurity band that would effectively lower the bandgap for optical absorption.[12] One of the most well-studied transition metal dopants in $SrTiO_3$ is Rh ($SrTiO_3$:Rh), which forms an electron donor level 2.4 eV below the conduction band minimum (CBM).[13] Doping with Rh, however, can introduce localized midgap acceptor states that act as efficient traps that severely reduce photocarrier lifetime, resulting in overall solar to hydrogen efficiencies well below[14] 1%. Co-doping with La has been proposed to reduce the traps and thus enhance the hydrogen evolution activity of this photocatalyst.[15] Indeed, in 2016, Wang et al. reported an efficiency of 1.1% for a Z-scheme system with La- and Rh-codoped $SrTiO_3$ hydrogen evolution reaction (HER) photo-

Received: February 14, 2023
Accepted: April 13, 2023
Published: May 10, 2023



ACS Publications

© 2023 American Chemical Society

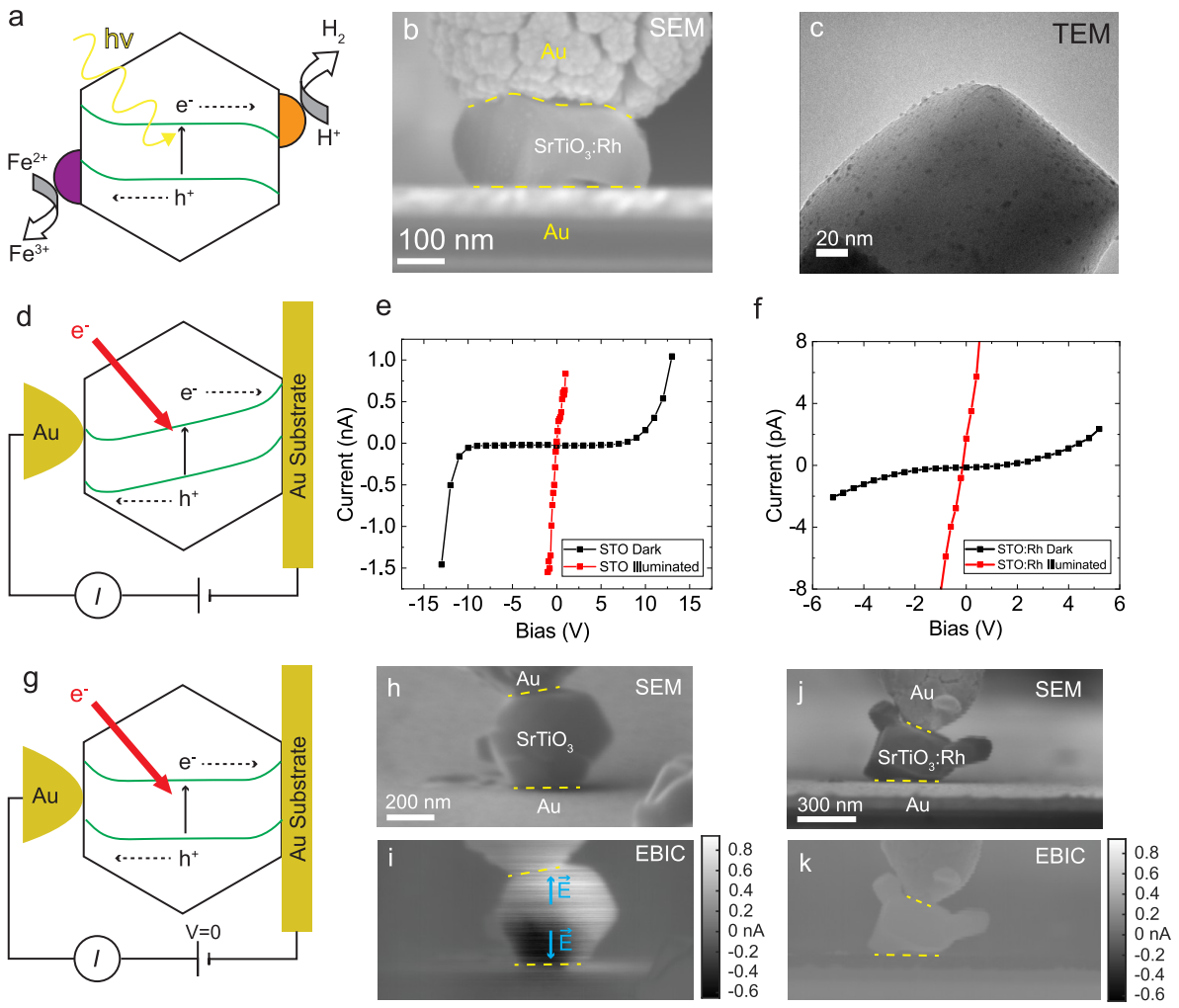


Figure 1. (a) Cartoon of a photocatalytic nanoparticle with band-bending (green lines) that separates charge to evolve hydrogen gas and oxidize a redox mediator (Fe^{2+}) in solution. (b) Gold nanoprobe makes electrical contact with a $SrTiO_3$:Rh nanoparticle within the SEM. (c) High-magnification TEM image of a $SrTiO_3$:Rh particle resolves 5 nm Pt cocatalysts on its surface. (d) Electrons injected by the primary electron beam create e−h pairs analogously to irradiation by light. (e,f) Bias-EBIC *I*−*V* curves become linear in both unintentionally doped (e) $SrTiO_3$ and Rh-doped $SrTiO_3$ (f) under e-beam illumination, and the photocarrier lifetimes are extracted assuming ideal photoconduction. (g) Absent applied bias, EBIC images acquired (i) from the same $SrTiO_3$ particle as (e,h) reveals strong built-in E fields at both Au-$SrTiO_3$ interfaces. Conversely, EBIC images acquired (k) from the Rh-doped $SrTiO_3$ particle of (f,j) no built-in E field due to a lack of free carriers. Dashed yellow lines are drawn on the SEM and EBIC images to mark the Au-$SrTiO_3$ interfaces.

catalyst nanoparticles paired with Mo-doped $BiVO_4$ oxygen evolution reaction (OER) photocatalysts.[16] Unfortunately, efficiencies substantially exceeding 1% have not been reported for $SrTiO_3$ since this study.[17]

The fact that STH efficiency for $SrTiO_3$:Rh photocatalysts is low despite substantial absorption in the visible (13% of photons from a solar blackbody approximation) points to either photocarrier transport or surface hydrogen evolution as the rate-limiting step. Poor transport characteristics have been shown to be the "Achilles heel" of otherwise promising water splitting materials such as hematite,[18−20] and recent results[21,22] doping $SrTiO_3$ nanoparticles with aluminum points to carrier transport as the rate-limiting step in $SrTiO_3$. The electronic impact of rhodium impurities has never been directly measured on individual photocatalysts, which is surprising since optically active impurities can also function as strong recombination centers.[23] Thus, the increased light absorptance (and corresponding increase in STH) from rhodium doping can be offset by a decreased charge-carrier lifetime and probability of reaching the photocatalyst surface.

In addition to a long carrier lifetime, another key requirement for efficient photoexcited electron−hole separation is an electric field within the photocatalyst that accelerates holes (electrons) in n-type (p-type) doped materials.[24] Internal electric fields imply space-charge layers, which can only form if the free carrier concentration is sufficiently large such that the Debye length in the semiconductor is well below the photocatalyst dimensions,[25] or $>10^{17}$ cm^{-3} for a $SrTiO_3$ particle with diameter of 400 nm. The importance of having a short Debye length, e.g., $L_D \ll D_{photocatalyst}$, to achieve efficient photocatalysis in colloidal semiconductor photocatalysts was recognized by Albery and Bartlett in their 1984 paper,[25] who laid out how the band bending (and the space-charge regions) needed to separate the photogenerated electrons and holes cannot be realized if the free carrier concentration, which dictates L_D, is too low. Unfortunately, while band bending and space charge regions are frequently

https://doi.org/10.1021/acsnano.3c01448
ACS Nano 2023, 17, 9405−9414

assumed to exist in nanoparticle photocatalysts, they are seldom measured. Here we apply a well-established method in semiconductor device characterization,[26] electron-beam induced current (EBIC) imaging, to directly map the space-charge regions in $SrTiO_3$ and $SrTiO_3$:Rh photocatalysts. We demonstrate that the addition of Rh essentially eliminates the space-charge regions, consistent with the formation of a large density of traps which drastically reduce the free carrier concentration.

The source of free electrons in unintentionally doped $SrTiO_3$ is often oxygen vacancies.[27,28] An oxygen vacancy contributes one free electron to the conduction band and a bound polaron with an energy 0.4 eV below the CBM.[27] A high concentration of oxygen vacancies ($>10^{17}$ cm^{-3}) is needed to establish internal electric fields within $SrTiO_3$ nanoparticles.[29] Even if the oxygen vacancy concentration is sufficiently large, the free electron concentration may be below this threshold if free electrons donated by oxygen vacancies are subsequently trapped within rhodium-induced traps. To the best of our knowledge, free carrier concentration of electrons in doped $SrTiO_3$ photocatalyst nanoparticles has never been measured.

To understand the origins of poor photocarrier separation and transport, we electrically probe individual $SrTiO_3$ and $SrTiO_3$:Rh photocatalyst nanoparticles using an environmental scanning electron microscope (SEM) retrofitted with nanomanipulators. We observe that carrier transport in $SrTiO_3$:Rh is dominated by trap-controlled space-charge-limited conduction (SCLC), in contrast to band transport in unintentionally doped $SrTiO_3$ nanoparticles. By analyzing current−voltage profiles measured under illumination with 1−10 keV electrons (which we call bias-EBIC to distinguish from unbiased EBIC images), we extract a photocarrier lifetime of 1.4 ps for $SrTiO_3$:Rh versus 71 ps for $SrTiO_3$. We use EBIC imaging to demonstrate that while space-charge regions are clearly observed in unintentionally doped $SrTiO_3$ nanoparticles, no such regions exist in $SrTiO_3$:Rh nanoparticles. The latter is consistent with very low free carrier concentration. We perform our measurements under both high vacuum and with 0.5 mbar of water vapor to demonstrate that water adsorption does not significantly change the carrier separation and transport characteristics. The short carrier lifetime and lack of built in electric fields to separate carriers explain why the external quantum yield (EQY) of $SrTiO_3$:Rh nanoparticles remains low, 1% measured at 405 nm, despite strong optical absorption at this wavelength. Based on our observation that $SrTiO_3$:Rh nanoparticles lack built-in electric fields, we propose that differences in mobility for electrons and holes drive the photocarrier separation necessary for photocatalytic activity.

RESULTS AND DISCUSSION

The unintentionally doped $SrTiO_3$ and $SrTiO_3$:Rh (1 at% Rh) nanoparticles, with and without Pt cocatalysts, were synthesized using a solid-state reaction (SSR) method previously described.[30] A transmission electron microscope (TEM) image of a typical $SrTiO_3$:Rh photocatalyst with Pt cocatalysts is shown in Figure 1c. The attenuation coefficient of 405 nm light through a $SrTiO_3$:Rh nanoparticle solution, as measured by UV−vis spectroscopy (Figure S2), is nearly five times higher than a suspension of similarly sized unintentionally doped $SrTiO_3$ nanoparticles. This result is in agreement with previous studies[30,31] which demonstrate that rhodium doping adds midgap traps that extend light absorption of $SrTiO_3$ into visible wavelengths.

Electronic transport measurements on individual nanoparticles are performed in an SEM retrofitted with nanoprobes and a heating stage (Figure 1d). The photocatalyst nanoparticles are dispersed from an aqueous mixture onto a Si/SiO_2 substrate coated with a Ti/Au (4 nm/100 nm) metallic film. Prior to dispersion, the substrate is washed with a poly(allylamine hydrochloride) solution (0.05 wt %) to improve nanoparticle adhesion. The Au-coated Si/SiO_2 serves as the back-contact, while a nanomanipulator-controlled, Au-coated W tip with a radius of 100 nm serves as the front contact.

A typical current−voltage ($I-V$) curve (Figure 1e) collected for an unintentionally doped $SrTiO_3$ nanoparticle under dark conditions (black trace) shows symmetric, nonlinear behavior. Further analysis reveals tunneling $I-V$ characteristics (Figure S3), typical of back-to-back Schottky contacts. When illuminated with a rastering 10 keV electron beam, the bias-EBIC current increases by a factor of $>10^3$ and becomes linear. The $SrTiO_3$:Rh similarly displays nonlinear dark $I-V$ characteristics (Figure 1f) but with a mechanism that is best described as trap-assisted space-charge-limited conduction (SCLC). SCLC is a bulk transport mechanism observed for semiconductors with very low free carrier concentrations, which we discuss in detail later. Illumination of the $SrTiO_3$:Rh nanoparticles with a 10 keV electron beam increases conductivity (G) of the $SrTiO_3$:Rh nanoparticles, analogously to photoconduction within a semiconductor[32] (Figure 1f, red curve). However, the bias-EBIC is lower than pure $SrTiO_3$ by at least 3 orders of magnitude (pA versus nA in Figure 1e,f). The carrier lifetime for unintentionally doped $SrTiO_3$ and $SrTiO_3$:Rh can be determined[32] from the bias-EBIC (the slope of a linear fit to the red points of Figure 1e) of the particle, $G = 8.5 \pm 0.1$ pS:

$$\frac{1}{\tau} = \frac{I_b A_p}{A_F} \frac{E_L}{3E_g} \frac{\mu}{GD^2} \tag{1}$$

where I_b is the beam current, reduced by the ratio of the projected particle area A_p to the frame area A_F since during 95% of its scan the beam is not incident on the particle. E_L is the energy loss (E_L = 2460 eV when calculated from the 14.2 MeV cm^2/g stopping power[33] of $SrTiO_3$ against 10 keV electrons) of the primary electron beam; $3E_g$ is the ionization energy[34] of E_g = 3.2 eV bandgap[35] $SrTiO_3$, μ is the electron mobility[36] of $SrTiO_3$ (~10 $cm^2/(V\ s)$), and D is the nanoparticle diameter. We note that the electron−hole (e−h) generation depth (based on the continuous slowing-down approximation) is calculated to be 870 nm, and therefore, e−h pairs are generated throughout the volume of a nanoparticle. For the D = 360 nm $SrTiO_3$:Rh particle shown in Figure 1j, a carrier lifetime of 1.4 ps is calculated, which is over an order of magnitude shorter than the 70 ps lifetime calculated for a similarly sized unintentionally doped $SrTiO_3$ nanoparticle (Figure 1h). This short carrier lifetime in $SrTiO_3$:Rh nanoparticles is likely due to rhodium midgap states functioning as recombination centers.[15,37] Our single-particle measurements of photocarrier lifetime in $SrTiO_3$:Rh nanoparticles agree within a factor of 2 with a previous lifetime measurement[38] of 2.8 ps made with time-resolved diffuse reflectance in $SrTiO_3$:Rh nanoparticle powder. Other studies in single-crystal $SrTiO_3$ have measured somewhat longer lifetimes[39,40] in the range of ps to ns, which is unsurprising due to

https://doi.org/10.1021/acsnano.3c01448
ACS Nano 2023, 17, 9405−9414

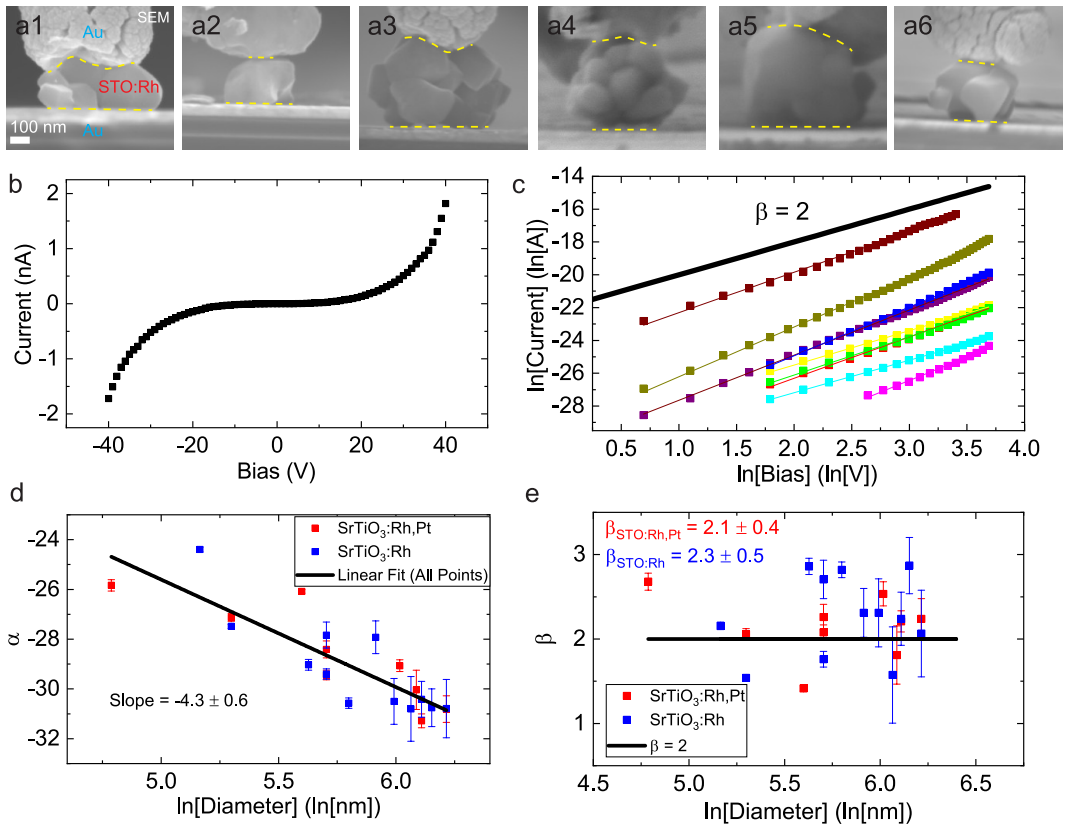


Figure 2. (a1−a6) SEM micrographs of representative $SrTiO_3$:Rh photocatalyst particles of varying sizes, with (a1−a3) and without Pt cocatalysts (a4−a6). Dashed-yellow lines are drawn on the SEM images to mark the Au-$SrTiO_3$:Rh interfaces. (b) In dark conditions, $I-V$ data are nonlinear, indicative of non-Ohmic transport. (c) Transport data from 9 nanoparticles can be linearized on a log−log scale, in agreement with SCLC conduction. (d) Constant field conductivity (α) exhibits a strong dependence on particle diameter, independent of the presence of a Pt cocatalyst. (e) Variable field conductivity (β) is, within its error bar, equal to the ideal value of 2 for both platinized and bare nanoparticles.

the higher quality of the single-crystal substrates used. We also note that long-lived electron traps in $SrTiO_3$ may have lifetimes in excess[37] of 10 s, but that here we are measuring the lifetime of free electrons promoted to the conduction band.

In a diffusive transport regime absent of an internal electric field, the calculated 1.4 ps lifetime of $SrTiO_3$:Rh corresponds to a very short diffusion length, $L = \sqrt{\mu k T \tau / e} = 5.9$ nm. Within a typical 170 nm radius particle, only the outer shell corresponding to 10% of its volume will generate photocarriers that contribute to electrochemical reactions at the surface. Thus, light absorbed within the inner ∼90% of the particle generates e−h pairs that rapidly recombine, prior to reaching the surface, limiting the EQY to a maximum of ∼10%. Assuming all other processes remain unchanged (and neglecting size-dependent Mie scattering), it follows that smaller particles should have higher EQY than larger particles, since the active volume of a smaller particle is a larger fraction of its total volume.

Although the photocarrier diffusion length of $SrTiO_3$:Rh is very short, a built-in electric field could still allow for efficient e−h separation. We use EBIC imaging to directly map built-in electric fields within the unintentionally doped and $SrTiO_3$:Rh (Figure 1g). EBIC imaging is a scanning electron probe technique that directly maps e−h separation efficiency within a semiconductor,[41−43] and has been used extensively to map space-charge regions within nanostructure with sub-10 nm spatial resolution.[41,44] Conventional secondary-electron images (Figure 1h,j) are acquired simultaneously with EBIC images (Figure 1i,k). Because the transimpedance current amplifier is connected to the gold substrate, a positive (negative) EBIC signal indicates electrons (holes) are moving preferentially toward the substrate and being collected by the inverting current amplifier. The location and direction of built-in electric fields can therefore be determined (cyan arrows in Figure 1i), since no external potential is applied. EBIC acquired from an unintentionally doped $SrTiO_3$ nanoparticle reveals strong contrast, and therefore built-in electric fields, at both $SrTiO_3$/Au interfaces (Figure 1i). The sign of the EBIC flips across the center of the nanoparticle, indicating that the built-in electric field changes direction. Based on the sign of the EBIC, the built-in electric field points from the $SrTiO_3$ to the gold, consistent with an n-type semiconductor with upward bending of the conduction band. Conversely, EBIC images of $SrTiO_3$:Rh nanoparticles at 0 V applied bias (Figure 1k) reveal a weak EBIC signal that is uniform across the particle, indicating that the built-in electric field is too weak to separate e−h pairs.

The lack of built-in electric field by rhodium doping can be explained by an absence of free carriers, consistent with bulk-limited SCLC transport. We note that conduction mechanisms that yield nonlinear characteristics can be broadly divided into interface-limited transport and bulk limited transport.[45−47] Interface-limited transport occurs when Schottky barriers or tunnel junctions form at the interfaces between the nanostructure and its contacts. Bulk-limited transport, on the

https://doi.org/10.1021/acsnano.3c01448
ACS Nano 2023, 17, 9405−9414

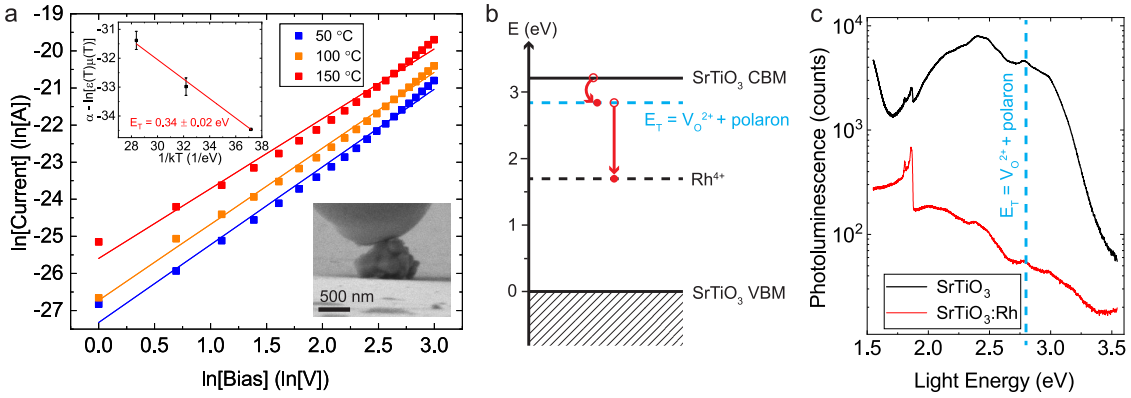


Figure 3. (a) Temperature-dependent conduction in a single $SrTiO_3$:Rh nanoparticle. (b) Energy band diagram for $SrTiO_3$:Rh with oxygen vacancy and Rh trap levels. (c) Photoluminescence taken from unintentionally doped and $SrTiO_3$:Rh nanoparticles confirms the presence of an oxygen vanacy trap at 2.8 eV above the valence band (marked with dashed-blue line). The PL intensity of $SrTiO_3$:Rh is 84 times lower, presumably due to nonradiative recombination via rhodium states.

other hand, is observed when the nanostructure has a high density of electronically active defects, forcing carriers to hop from trap-to-trap, or when the current density becomes space-charge-limited due to a low number of free carriers.[48] Fitting our experimental data to the various mechanisms (Figure S4), we find that bulk-limited single-trap SCLC provides a better fit compared to interface-limited Schottky or tunnel junction type mechanisms.

SCLC conduction is a bulk-limited transport mechanism of the form[49,50]

$$I = \frac{9A\epsilon_r\epsilon_0\mu V^2}{8D^3}\frac{N_c}{N_t}e^{-E_T/kT} \tag{2}$$

where I is the measured current, $\epsilon_r = 300$ is the relative permittivity[51] of the $SrTiO_3$, ϵ_0 is the permittivity of vacuum, μ is the bulk electron mobility[36] (10 $cm^2/V\,s$), A is the contact area, D is the nanoparticle diameter, E_T is the trap energy below the conduction band minimum (CBM), N_T is the trap density, N_C is the density of states in the conduction band, k is the Boltzmann constant, T is temperature in Kelvin, and V is the applied bias. States in the conduction band are likely due to oxygen vacancies in the $SrTiO_3$, which act as n-type dopants.[21] The above expression can be linearized on a log−log plot as $\ln[I] = \alpha + \beta \ln[V]$, where $\alpha = \ln\left[\frac{9A\epsilon\mu N_C}{8D^3N_T}\right] - \frac{E_T}{kT}$ and $\beta = 2$. Current−voltage measurements collected for 9 particles (Figure 2c) are linearized on a log−log plot, in agreement with SCLC transport. The mean value of β for this collection of 9 nanoparticles is 2.1 ± 0.4, equal to the ideal value of 2 to within the standard deviation of the data set.

Smaller-diameter nanoparticles have dramatically higher conductivity compared to those with a larger-diameter, in agreement with SCLC transport. Conductance (α) at 1 V bias versus particle diameter is plotted on a log−log scale (Figure 2d) and fit to a line with a slope of −4.3 ± 0.6. This diameter dependence is stronger than expected for ideal SCLC, which has a D^{-3} dependence on diameter that would correspond to a slope of −3 on the plot in Figure 2d. This discrepancy may be due to the polycrystalline morphology of the $SrTiO_3$ nanoparticles, as larger particles are observed to have more grain boundaries than smaller particles, which may lower conductance due to grain-boundary resistance. The larger conductance observed for smaller diameter photocatalysts also indicates that surface defects are not the dominant trap of free carriers. If this were the case, the conductance would decrease as diameter decreases, due to an increase in surface-to-volume ratio, as previously observed for III−V semiconductor nanostructures.[52]

The addition of Pt cocatalysts to the surface of the $SrTiO_3$:Rh particles has an insignificant effect on carrier transport, as seen in Figure 2 d,e, where transport parameters (α and β) extracted from SCLC fits are plotted for nine $SrTiO_3$:Rh nanoparticles with Pt cocatalysts alongside 12 bare $SrTiO_3$:Rh nanoparticles. The slopes (Figure 2d) of the α versus D plots, along with mean values of β, of the $SrTiO_3$:Rh nanoparticles with and without Pt cocatalysts overlap within their respective error bars. This result is not surprising given that the ∼5 nm diameter of the Pt cocatalysts is much smaller than a typical 400 nm diameter $SrTiO_3$ particle, meaning that the 1-D Schottky model will not be accurate.[53−55] A better model for electrostatic screening in this system is a point charge resting on the surface of a semiconductor,[53−55] which is related to the "pinch-off" effect describing an inhomogeneity within an ideal Schottky contact.[56,57] This "pinch-off" effect limits the size of the space-charge region (and potential barrier) beneath small Schottky contacts to the diameter of the contact.[56] Therefore, regardless of free carrier concentration within the $SrTiO_3$, the ∼5 nm diameter cocatalysts cannot form a space-charge layer more than approximately 5 nm from the surface.

Temperature-dependent transport measurements taken on a single nanoparticle (Figure 3a) demonstrate increasing conductivity (α) with increasing temperature, consistent with the exponential temperature dependence of the single-trap SCLC model eq 2. A linear regression (Figure 3a, inset) of α versus $1/kT$ yields a trap depth of $E_T = 0.34 \pm 0.02$ eV below the CBM. According to Janotti et al.,[27] oxygen vacancies in $SrTiO_3$ can trap two polarons localized on neighboring Ti atoms. The first polaron is easily ionized at room temperature and becomes a free electron in the conduction band, while the second polaron remains trapped in a state (V_O^{2+}) 0.4 eV below the CBM (Figure 3b). This state corresponds to an optical transition of 2.8 eV (0.4 eV less than the 3.2 eV bandgap[35] of $SrTiO_3$). We observe this state as a peak in photoluminescence (PL) spectra in both unintentionally doped and $SrTiO_3$:Rh nanoparticles (Figure 3c), confirming this state is not due to rhodium. The energy of this state (0.4 eV below the CBM) is

https://doi.org/10.1021/acsnano.3c01448
ACS Nano 2023, 17, 9405−9414

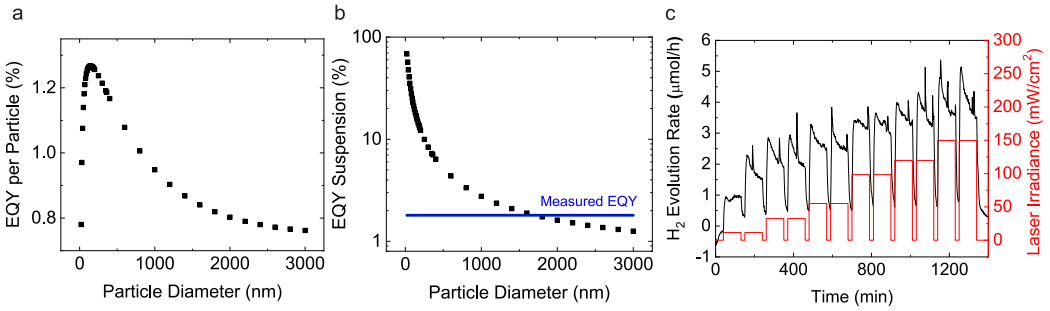


Figure 4. (a) EQY for 405 nm light is simulated for a single $SrTiO_3$:Rh nanoparticle. (b) Total EQY for 405 nm light of a $SrTiO_3$:Rh (0.5 g/L) suspension is simulated versus particle diameter. (c) Mass spectroscopic signal at m/z = 2 corresponding to H_2 evolved during chopped light irradiation (405 nm) of $SrTiO_3$:Rh particles (0.5 g/L) with Pt cocatalysts in an aqueous CH_3OH solution (10% v/v).

close enough to the electronically measured trap energy (E_T = 0.34 ± 0.02), to conclude this trap is responsible for SCLC. The very low free carrier concentration we observe in $SrTiO_3$:Rh is likely due to the empty Rh^{4+} states[58] (1.7 eV below the CBM) trapping the free carriers donated by oxygen vacancies, while the remaining electrons, trapped in the form of small polarons, must overcome the 0.34 eV activation barrier for conduction. From eq 2, using a conduction band density of states[29] of N_C = 7.9 × 10^{20} cm^{-3}, an oxygen vacancy concentration of N_T = 2.2 × 10^{20} cm^{-3} is calculated. At room temperature, the probability that a polaron will escape to the conduction band is $p = \frac{N_C}{N_T}\exp[-E_T/kT]$ = 8.9 × 10^{-6}. The effective free carrier concentration is thus reduced by this factor to 2.0 × 10^{15} cm^{-3}, more than 4 orders of magnitude smaller than the oxygen vacancy concentration.

The bulk nonradiative carrier lifetime extracted from the $SrTiO_3$ powder PL data (Figure 3c) is consistent with bias-EBIC measurements made on individual nanoparticles. The intensity (I_{PL}) of a PL peak is proportional to the ratio of the radiative carrier recombination rate,[59] R_{rad}, to the total recombination rate, $R_{tot} = R_{rad} + R_{nonrad}$, where R_{nonrad} is the nonradiative recombination rate. Therefore, $I_{PL} \propto R_{rad}/R_{tot} = \tau_{rad}^{-1}/\tau_{tot}^{-1}$. Assuming that $\tau_{rad} \gg \tau_{nonrad}$, the intensity of a peak is proportional to τ_{nonrad}/τ_{rad}. Rhodium doping decreases the intensity of the V_O^{2+} polaron peak by a factor of 84. Assuming τ_{rad} is unaffected by rhodium midgap states, τ_{nonrad} will be reduced by this same factor, which agrees well with our previous single-particle betaconduction measurements. Although characterizing individual nanoparticles with PL is difficult due to their small (subwavelength) diameter, other techniques such as SEM cathodoluminescence could provide relative photocarrier lifetime measurements of individual photocatalyst particles.

Given our measurement of 1.4 ps photocarrier lifetime, we simulate EQY for a solution of $SrTiO_3$ nanoparticles, and find that smaller particles will yield higher EQY. Photocarriers can diffuse an average of 5.9 nm before recombining; therefore, the active volume of a nanoparticle will be a spherical shell of width 5.9 nm extending from the surface. As a function of particle diameter, EQY per particle (illuminated with 405 nm light) will initially increase due to increased light absorption (Figure 4a), plateau at ∼150 nm diameter, and decrease at larger diameters since the fraction of a particle's active volume shrinks. Within a suspension of particles (0.5 g/L), total EQY will decrease monotonically with diameter (Figure 4b) since the mass density of the solution (and therefore total light absorption) is held constant. To experimentally validate these simulations, we suspend $SrTiO_3$:Rh/Pt nanoparticles (0.5 g/L) in a solution of 10% v/v methanol (aq) and $SrTiO_3$:Rh and irradiate with a 405 nm laser. Mass spectroscopy is used to measure H_2 evolution, with an EQY 1.8 ± 0.4% under 11.6 mW/cm^2 (Figure 4c), which is consistent with performance reported in previous studies of similarly prepared photocatalysts.[6] The measured EQY of 1.8 ± 0.4% corresponds to a particle diameter of 1.8 μm, larger than our SEM-measured average particle diameter of ∼400 nm. This result suggests that either nanoparticles are clustering within the solution, lowering the observed EQY, or that there are other inefficiencies in the water-splitting process which are not accounted for in our model.

The space-charge region of a semiconductor nanoparticle contacting metal (or surrounded by electrolyte) is geometrically limited when the radius of the particle is less than the space charge width, (W) within the semiconductor.[25] In the 1-D Schottky model, the space-charge width is equal to $W = \sqrt{\frac{2\epsilon}{qN_C}\phi}$. For unintentionally doped $SrTiO_3$ nanoparticles, the free carrier density will be simply the oxygen vacancy concentration (N_C = 2.2 × 10^{20} cm^{-3}) and the barrier height was measured (Figure S3) via transport (ϕ = 0.11 eV). Using these two values in the 1-D Schottky model yields a space-charge width of 4 nm, well below the diameter of a nanoparticle. However, the free carrier concentration in $SrTiO_3$:Rh nanoparticles is dramatically reduced to 2.0 × 10^{15} cm^{-3}, extending the width of the space-charge region to 1.3 μm, approximately three times as large as the diameter of an average nanoparticle. In this regime, the maximum built-in potential is limited (Supporting Information) to $V_S = D^2qN_C/24\epsilon$ = 0.8 mV, over an order of magnitude smaller than room temperature thermal voltage. It should be noted that this expression for maximum built-in potential also applies to free holes within a p-type semiconductor. Rhodium atoms within $SrTiO_3$ can introduce free holes, converting $SrTiO_3$ to a p-type semiconductor.[13] If the free hole concentration is sufficiently high, the space-charge region width will be smaller than the nanoparticle diameter, resulting in downward band-bending.[13,37] In our $SrTiO_3$:Rh nanoparticles, we calculate the oxygen vacancy concentration (2.2 × 10^{20} cm^{-3}) to be higher than the Rh dopant concentration (1.6 × 10^{20} cm^{-3}). Even if each rhodium atom donated a free hole to the valence band, due to dopant compensation, these nanoparticles would still be n-type due to a higher concentration of oxygen vacancies. We emphasize that although the oxygen vacancy concentration is high within these $SrTiO_3$:Rh nanoparticles, we nevertheless measure photocatalytic hydrogen evolution (Figure 4c).

https://doi.org/10.1021/acsnano.3c01448
ACS Nano 2023, 17, 9405−9414

The built-in potential of a $SrTiO_3$:Rh nanoparticle does not depend on the barrier height between the nanoparticle and its contact, and thus even if nanoparticles are submerged in an electrolyte we expect the built-in potential will still be 0.8 mV. Indeed, single-particle transport measurements of $SrTiO_3$:Rh with Pt cocatalysts with an atmosphere of 0.5 mbar of water vapor show no significant change in either dark current or bias-EBIC compared to a high-vacuum environment (Figure S8). This result is consistent with our hypothesis that bulk rather than surface states are responsible for trapping free carriers and SCLC conduction in Rh-doped $SrTiO_3$.

A recent demonstration[21] of near 100% EQY for $SrTiO_3$:Al is consistent with our findings, since Al does not appear to introduce traps in $SrTiO_3$, thereby allowing for band-bending and efficient e−h separation. Unfortunately, light absorption of $SrTiO_3$:Al does not extend into visible wavelengths, and therefore its overall STH efficiency is still low. A new dopant is needed, that combines the long lifetimes of aluminum with the good visible-light absorption of rhodium, to achieve efficient solar-powered water splitting.

It is perhaps surprising that even modest e−h separation in $SrTiO_3$:Rh nanoparticles can occur without an internal electric field, since one might expect charge carriers in a photogenerated e−h pair to be attracted to each other and immediately recombine. However, $SrTiO_3$ (ϵ_r = 300, m_e^* = $10m_0$, m_H^* = $10m_0$) will efficiently screen[51,60,61] Coulomb attraction between an electron and hole, resulting in a low Wannier exciton energy[62] of 0.8 meV. This energy is well below room temperature kT, implying photogenerated carriers will freely diffuse within the nanoparticle. However, the electron mobility[36] in $SrTiO_3$ (~10 $cm^2/(V\ s)$) greatly exceeds that of holes[63] (~5×10^{-3} $cm^2/(V\ s)$). This disparity suggests that following optical absorption, photoexcited electrons will diffuse to the $SrTiO_3$/Pt or $SrTiO_3$/electrolyte interfaces well ahead of the holes. These electrons can then drive proton reduction reactions via hydrogen adsorption onto the Pt cocatalysts (Volmer step), and/or by facilitating hydrogen evolution through the Heyrovsky step at the same Pt sites. Alternatively, the electrons can react with spilled over H atoms and protons on the $SrTiO_3$ surface, as previously observed[64] for Si/SiO_2 photocathodes decorated with Pt cocatalysts. Once reduction reactions consume an electron, the $SrTiO_3$:Rh nanoparticle has a net positive charge, which favors an oxidation reaction to eliminate the excess charge.

CONCLUSIONS

In summary, we have electrically probed individual $SrTiO_3$ nanoparticles, with and without rhodium doping, and found that rhodium-induced traps decrease photocarrier lifetime by over an order of magnitude and free carrier concentration by over 10^5. Both of these factors dramatically reduce the maximum achievable EQY. Low free carrier concentration reduces the electric field due to the band-bending needed to effectively separate and transport the photocarriers to the nanoparticle surface. The maximum EQY is instead limited by the electron diffusion length, which is small due to a short photocarrier lifetime. In this regime of sub-ns photocarrier lifetime the standard drift-diffusion model is not accurate since more than one electron−hole pair is not present within a nanoparticle at a given time. A new model of quantized charge separation is needed, that takes into account the large difference in mobility between electrons and holes in $SrTiO_3$. Future research in $SrTiO_3$ nanoparticles for water splitting should search for either (i) a codopant to passivate Rh-induced traps or (ii) a new dopant that creates midgap states to absorb visible light, without significantly degrading photocarrier lifetime.

EXPERIMENTAL SECTION

Electrical measurements are performed within an FEI Nova NanoSEM 230, equipped with nanomanipulators and electrical feedthroughs. Transport measurements were acquired with a Keithley 237 sourcemeter. EBIC images were acquired with a Keithley 428 transimpedance amplifier set to 10^9 V/A.

To assess the photocatalytic activity of the Pt/$SrTiO_3$:Rh nanoparticles, a Hiden HPR-20 EGA mass spectrometer/residual gas analyzer (MS/RGA) system was used to continuously monitor the gas composition of the headspace of photocatalyst solution (0.5 mg of nanoparticles suspended in 1 mL of 10% v/v aqueous CH_3OH solution) in the reactor cuvette. A Thorlabs L405G1 laser diode was used as the light source. The carrier gas used was argon (99.999% ultrahigh purity), and a calibration process of injecting a known amount of hydrogen (99.999% ultrahigh purity) gas into the reactor cuvette was performed at the end of the MS experiment (data not shown). EQY was calculated using m/z = 2 (hydrogen) partial pressure readings after system reached quasi-steady-state near the end of each light on period. Caution was taken when selecting the m/z = 2 partial pressure for EQY calculations. Notably, due to the mechanical energy introduced by the stir bar and local heating by the laser, water molecules can vaporize from liquid phase into gas phase, causing sporadic spikes in Figure 4c data (16 other mass to charge ratios were also measured, water m/z = 18 correlated best to the spikes). For all EQY calculations, m/z = 2 pressure readings were taken when m/z = 18 (water) pressure readings were stable/at steady state to minimize the contribution of water in hydrogen signal. The reported 1.8% EQY is for the lowest light intensity, as light intensity further increases, QY decreases.

X-ray photoelectron spectroscopy (XPS) measurements were performed using a Kratos AXIS Supra photoelectron spectrometer with monochromic Al Kα radiation (supplementary Figure S9). CasaXPS software was used for XPS data analysis. To minimize sample charging, a flood gun was used. To correct for any charges on the sample that the flood gun was unable to neutralize, all samples were referenced to the adventitious carbon 1s peak at a binding energy of 284.8 eV. Using a Shirley type background, all data was fitted using a Gaussian−Lorentzian (50:50) line shape. For spin doublet peaks, based on total angular momentum (j) values, peak area ratio restrictions were applied.

ASSOCIATED CONTENT

Supporting Information

The Supporting Information is available free of charge at https://pubs.acs.org/doi/10.1021/acsnano.3c01448.

Figures S1−S9, simulated EQY in a nanoparticle solution, barrier height measurement in undoped $SrTiO_3$ nanoparticles, calculation of maximum built-in potential for a nanoparticle, optical absorption measurements, additional transport data in water vapor, bias-EBIC data under low-illumination conditions, additional EBIC data, and XPS characterization of $SrTiO_3$ nanoparticles (PDF)

AUTHOR INFORMATION

Corresponding Author

A. Alec Talin − *Materials Physics Department, Sandia National Laboratories, Livermore, California 94550, United States;* orcid.org/0000-0002-1102-680X; Email: aatalin@sandia.gov

https://doi.org/10.1021/acsnano.3c01448
ACS Nano 2023, 17, 9405−9414

Authors

Brian Zutter − *Materials Physics Department, Sandia National Laboratories, Livermore, California 94550, United States;* orcid.org/0000-0002-3604-5791

Zejie Chen − *Department of Chemistry, University of California, Irvine, California 92697, United States*

Luisa Barrera − *Department of Mechanical Engineering, University of Michigan, Ann Arbor, Michigan 48109, United States*

William Gaieck − *Department of Chemistry, University of California, Irvine, California 92697, United States*

Aliya S. Lapp − *Materials Physics Department, Sandia National Laboratories, Livermore, California 94550, United States*

Kenta Watanabe − *Department of Applied Chemistry, Faculty of Science, Tokyo University of Science, Tokyo 162-8601, Japan;* orcid.org/0000-0003-0827-7381

Akihiko Kudo − *Department of Applied Chemistry, Faculty of Science, Tokyo University of Science, Tokyo 162-8601, Japan*

Daniel V. Esposito − *Department of Chemical Engineering, Columbia University, New York, New York 10027, United States;* orcid.org/0000-0002-0550-801X

Rohini Bala Chandran − *Department of Mechanical Engineering, University of Michigan, Ann Arbor, Michigan 48109, United States;* orcid.org/0000-0002-2745-8893

Shane Ardo − *Department of Chemistry, Department of Materials Science and Engineering, and Department of Chemistry and Biomolecular Engineering, University of California, Irvine, California 92697, United States;* orcid.org/0000-0001-7162-6826

Complete contact information is available at: https://pubs.acs.org/10.1021/acsnano.3c01448

Author Contributions

A.T. conceived the idea. K.W. and A.K. synthesized the photocatalytic $SrTiO_3$:Rh nanoparticles. Z.C. and S.A. measured the EQY of $SrTiO_3$:Rh nanoparticles in solution. L.B. and R.B.C. performed EQY simulations of $SrTiO_3$:Rh nanoparticles in solution. W.G. acquired TEM on individual nanoparticles. B.Z. and A.L. performed electrical and optical characterization. B.Z., L.B., R.B.C., and A.T. analyzed results. B.Z. and A.T. wrote the paper. All authors discussed experiments and the final manuscript.

Notes

The authors declare no competing financial interest.

ACKNOWLEDGMENTS

The authors thank I. Tran (UC Irvine) for guidance in X-ray photoelectron spectroscopy data analysis. XPS work was performed using instrumentation funded in part by the National Science Foundation Major Research Instrumentation Program under Grant No. CHE-1338173. This work was supported by the U.S. Department of Energy (DOE), Office of Energy Efficiency and Renewable Energy (EERE), Hydrogen and Fuel Cell Technologies Office (HFTO), and specifically the HydroGEN Advanced Water Splitting Materials Consortium, established as part of the Energy Materials Network under this same office (Award DE-EE0008838). Analysis of the photocarrier concentration was supported by the Ensembles of Photosynthetic Nanoreactors (EPN), an Energy Frontier Research Center funded by the U.S. Department of Energy, Office of Science under Award Number DE-SC0023431. The authors acknowledge the use of facilities and instrumentation at the UC Irvine Materials Research Institute (IMRI), which is supported in part by the National Science Foundation through the UC Irvine Materials Research Science and Engineering Center (DMR-2011967). Sandia National Laboratories is a multimission laboratory managed and operated by National Technology and Engineering Solutions of Sandia, LLC., a wholly owned subsidiary of Honeywell International, Inc., for the U.S. Department of Energy's National Nuclear Security Administration under contract DE-NA0003525. The views expressed in this article do not necessarily represent the views of the U.S. Department of Energy or the United States Government.

REFERENCES

(1) Chen, S.; Takata, T.; Domen, K. Particulate photocatalysts for overall water splitting. *Nature Reviews Materials* **2017**, *2*, 17050.

(2) Pinaud, B. A.; Benck, J. D.; Seitz, L. C.; Forman, A. J.; Chen, Z.; Deutsch, T. G.; James, B. D.; Baum, K. N.; Baum, G. N.; Ardo, S.; Wang, H.; Miller, E.; Jaramillo, T. F. Technical and economic feasibility of centralized facilities for solar hydrogen production via photocatalysis and photoelectrochemistry. *Energy Environ. Sci.* **2013**, *6*, 1983−2002.

(3) James, B. D.; Baum, G. N.; Perez, J.; Baum, K. N. *Technoeconomic Analysis of Photoelectrochemical (PEC) Hydrogen Production*, 2009; Directed Technologies, Inc., https://www.osti.gov/biblio/1218403 (accessed April 11, 2023).

(4) Goto, Y.; Hisatomi, T.; Wang, Q.; Higashi, T.; Ishikiriyama, K.; Maeda, T.; Sakata, Y.; Okunaka, S.; Tokudome, H.; Katayama, M.; Akiyama, S.; Nishiyama, H.; Inoue, Y.; Takewaki, T.; Setoyama, T.; Minegishi, T.; Takata, T.; Yamada, T.; Domen, K. A Particulate PhotocatalystWater-Splitting Panel for Large-Scale Solar Hydrogen Generation. *Joule* **2018**, *2*, 509−520.

(5) Bala Chandran, R.; Breen, S.; Shao, Y.; Ardo, S.; Weber, A. Z. Evaluating particlesuspension reactor designs for Z-scheme solar water splitting via transport and kinetic modeling. *Energy Environ. Sci.* **2018**, *11*, 115−135.

(6) Fabian, D. M.; Hu, S.; Singh, N.; Houle, F. A.; Hisatomi, T.; Domen, K.; Osterloh, F. E.; Ardo, S. Particle suspension reactors and materials for solar-driven water splitting. *Energy Environ. Sci.* **2015**, *8*, 2825−2850.

(7) Nishiyama, H.; Yamada, T.; Nakabayashi, M.; Maehara, Y.; Yamaguchi, M.; Kuromiya, Y.; Nagatsuma, Y.; Tokudome, H.; Akiyama, S.; Watanabe, T.; Narushima, R.; Okunaka, S.; Shibata, N.; Takata, T.; Hisatomi, T.; Domen, K. Photocatalytic solar hydrogen production from water on a 100-m2 scale. *Nature* **2021**, *598*, 304−307.

(8) Ager, J. W.; Shaner, M. R.; Walczak, K. A.; Sharp, I. D.; Ardo, S. Experimental demonstrations of spontaneous, solar-driven photoelectrochemical water splitting. *Energy Environ. Sci.* **2015**, *8*, 2811−2824.

(9) Wrighton, M. S.; Ellis, A. B.; Wolczanski, P. T.; Morse, D. L.; Abrahamson, H. B.; Ginley, D. S. Strontium titanate photoelectrodes. Efficient photoassisted electrolysis of water at zero applied potential. *J. Am. Chem. Soc.* **1976**, *98*, 2774−2779.

(10) Mavroides, J. G.; Kafalas, J. A.; Kolesar, D. F. Photoelectrolysis of water in cells with $SrTiO_3$ anodes. *Appl. Phys. Lett.* **1976**, *28*, 241−243.

(11) Watanabe, T.; Fujishima, A.; Honda, K.-i. Photoelectrochemical Reactions at $SrTiO_3$ Single Crystal Electrode. *Bull. Chem. Soc. Jpn.* **1976**, *49*, 355−358.

(12) Wang, Q.; Domen, K. Particulate Photocatalysts for Light-Driven Water Splitting: Mechanisms, Challenges, and Design Strategies. *Chem. Rev.* **2020**, *120*, 919−985.

(13) Iwashina, K.; Kudo, A. Rh-Doped $SrTiO_3$ Photocatalyst Electrode Showing Cathodic Photocurrent for Water Splitting under Visible-Light Irradiation. *J. Am. Chem. Soc.* **2011**, *133*, 13272−13275.

(14) Masood, H.; Toe, C. Y.; Teoh, W. Y.; Sethu, V.; Amal, R. Machine Learning for Accelerated Discovery of Solar Photocatalysts. *ACS Catal.* **2019**, *9*, 11774−11787.
(15) Modak, B.; Ghosh, S. K. Exploring the Role of La Codoping beyond Charge Compensation for Enhanced Hydrogen Evolution by Rh−$SrTiO_3$. *J. Phys. Chem. B* **2015**, *119*, 11089−11098.
(16) Wang, Q.; Hisatomi, T.; Jia, Q.; Tokudome, H.; Zhong, M.; Wang, C.; Pan, Z.; Takata, T.; Nakabayashi, M.; Shibata, N.; Li, Y.; Sharp, I. D.; Kudo, A.; Yamada, T.; Domen, K. Scalable water splitting on particulate photocatalyst sheets with a solar-tohydrogen energy conversion efficiency exceeding 1%. *Nat. Mater.* **2016**, *15*, 611−615.
(17) Schumacher, L.; Marschall, R. Recent Advances in Semiconductor Heterojunctions and Z-Schemes for Photocatalytic Hydrogen Generation. *Topics in Current Chemistry* **2022**, *380*, 53.
(18) Sivula, K.; Zboril, R.; Le Formal, F.; Robert, R.; Weidenkaff, A.; Tucek, J.; Frydrych, J.; Grätzel, M. Photoelectrochemical Water Splitting with Mesoporous Hematite Prepared by a Solution-Based Colloidal Approach. *J. Am. Chem. Soc.* **2010**, *132*, 7436−7444.
(19) Cherepy, N. J.; Liston, D. B.; Lovejoy, J. A.; Deng, H.; Zhang, J. Z. Ultrafast Studies of Photoexcited Electron Dynamics in - and -Fe_2O_3 Semiconductor Nanoparticles. *J. Phys. Chem. B* **1998**, *102*, 770−776.
(20) Bohn, C. D.; Agrawal, A. K.; Walter, E. C.; Vaudin, M. D.; Herzing, A. A.; Haney, P. M.; Talin, A. A.; Szalai, V. A. Effect of Tin Doping on -Fe_2O_3 Photoanodes for Water Splitting. *J. Phys. Chem. C* **2012**, *116*, 15290−15296.
(21) Zhao, Z.; Goncalves, R. V.; Barman, S. K.; Willard, E. J.; Byle, E.; Perry, R.; Wu, Z.; Huda, M. N.; Moule, A. J.; Osterloh, F. E. Electronic structure basis for enhanced overall water splitting photocatalysis with aluminum doped $SrTiO_3$ in natural sunlight. *Energy Environ. Sci.* **2019**, *12*, 1385−1395.
(22) Takata, T.; Domen, K. Defect Engineering of Photocatalysts by Doping of Aliovalent Metal Cations for Efficient Water Splitting. *J. Phys. Chem. C* **2009**, *113*, 19386−19388.
(23) Serpone, N.; Emeline, A. V.; Ryabchuk, V. K.; Kuznetsov, V. N.; Artem'ev, Y. M.; Horikoshi, S. Why do Hydrogen and Oxygen Yields from Semiconductor-Based Photocatalyzed Water Splitting Remain Disappointingly Low? Intrinsic and Extrinsic Factors Impacting Surface Redox Reactions. *ACS Energy Letters* **2016**, *1*, 931−948.
(24) Calarco, R.; Stoica, T.; Brandt, O.; Geelhaar, L. Surface-induced effects in GaN nanowires. *J. Mater. Res.* **2011**, *26*, 2157−2168.
(25) Albery, W. J.; Bartlett, P. N. The Transport and Kinetics of Photogenerated Carriers in Colloidal Semiconductor Electrode Particles. *J. Electrochem. Soc.* **1984**, *131*, 315.
(26) Schroder, D. *Semiconductor Material and Device Characterization*, 3rd ed.; Wiley: Hoboken, NJ, 2006; p 416.
(27) Janotti, A.; Varley, J. B.; Choi, M.; Van de Walle, C. G. Vacancies and small polarons in $SrTiO_3$. *Phys. Rev. B* **2014**, *90*, No. 085202.
(28) Herranz, G.; Basletić, M.; Bibes, M.; Carrétéro, C.; Tafra, E.; Jacquet, E.; Bouzehouane, K.; Deranlot, C.; Hamzić, A.; Broto, J.-M.; Barthélémy, A.; Fert, A. High Mobility in $LaAlO_3/SrTiO_3$ Heterostructures: Origin, Dimensionality, and Perspectives. *Phys. Rev. Lett.* **2007**, *98*, 216803.
(29) Takata, T.; Jiang, J.; Sakata, Y.; Nakabayashi, M.; Shibata, N.; Nandal, V.; Seki, K.; Hisatomi, T.; Domen, K. Photocatalytic water splitting with a quantum efficiency of almost unity. *Nature* **2020**, *581*, 411−414.
(30) Konta, R.; Ishii, T.; Kato, H.; Kudo, A. Photocatalytic Activities of Noble Metal Ion Doped $SrTiO_3$ under Visible Light Irradiation. *J. Phys. Chem. B* **2004**, *108*, 8992−8995.
(31) Kawasaki, S.; Nakatsuji, K.; Yoshinobu, J.; Komori, F.; Takahashi, R.; Lippmaa, M.; Mase, K.; Kudo, A. Epitaxial Rh-doped $SrTiO_3$ thin film photocathode for water splitting under visible light irradiation. *Appl. Phys. Lett.* **2012**, *101*, No. 033910.
(32) Quimby, R. *Photonics and Lasers*; Wiley: Hoboken, NJ, 2006; p 239.
(33) Berger, M.; Coursey, J.; Zucker, M.; Chang, J. *ESTAR, PSTAR, and ASTAR: Computer Programs for Calculating Stopping-Power and Range Tables for Electrons, Protons, and Helium Ions (version 1.2.3)*, 2005; National Institute of Standards and Technology, https://physics.nist.gov/PhysRefData/Star/Text/ESTAR.html (accessed April 11, 2023).
(34) Klein, C. A. Bandgap Dependence and Related Features of Radiation Ionization Energies in Semiconductors. *J. Appl. Phys.* **1968**, *39*, 2029−2038.
(35) Reihl, B.; Bednorz, J. G.; Müller, K. A.; Jugnet, Y.; Landgren, G.; Morar, J. F. Electronic structure of strontium titanate. *Phys. Rev. B* **1984**, *30*, 803−806.
(36) Spinelli, A.; Torija, M. A.; Liu, C.; Jan, C.; Leighton, C. Electronic transport in doped $SrTiO_3$: Conduction mechanisms and potential applications. *Phys. Rev. B* **2010**, *81*, 155110.
(37) Moss, B.; Wang, Q.; Butler, K. T.; Grau-Crespo, R.; Selim, S.; Regoutz, A.; Hisatomi, T.; Godin, R.; Payne, D. J.; Kafizas, A.; Domen, K.; Steier, L.; Durrant, J. R. Linking in situ charge accumulation to electronic structure in doped $SrTiO_3$ reveals design principles for hydrogen-evolving photocatalysts. *Nat. Mater.* **2021**, *20*, 511−517.
(38) Murthy, D. H. K.; Matsuzaki, H.; Wang, Q.; Suzuki, Y.; Seki, K.; Hisatomi, T.; Yamada, T.; Kudo, A.; Domen, K.; Furube, A. Revealing the role of the Rh valence state, La doping level and Ru cocatalyst in determining the H 2 evolution efficiency in doped SrTiO 3 photocatalysts. *Sustainable Energy & Fuels* **2019**, *3*, 208−218.
(39) Rubano, A.; Ciccullo, F.; Paparo, D.; Miletto Granozio, F.; Scotti di Uccio, U.; Marrucci, L. Photoluminescence dynamics in strontium titanate. *J. Lumin.* **2009**, *129*, 1923−1926.
(40) Kanemitsu, Y.; Yamada, Y. Light emission from $SrTiO_3$. *physica status solidi (b)* **2011**, *248*, 416−421.
(41) Zutter, B. T.; Kim, H.; Hubbard, W. A.; Ren, D.; Mecklenburg, M.; Huffaker, D.; Regan, B. Mapping Charge Recombination and the Effect of Point-Defect Insertion in GaAs Nanowire Heterojunctions. *Physical Review Applied* **2021**, *16*, No. 044030.
(42) Reimer, L. *Scanning Electron Microscopy*, 2nd ed.; Springer-Verlag: Berlin, 1998.
(43) Poplawsky, J. D.; Li, C.; Paudel, N. R.; Guo, W.; Yan, Y.; Pennycook, S. J. Nanoscale doping profiles within CdTe grain boundaries and at the CdS/CdTe interface revealed by atom probe tomography and STEM EBIC. *Sol. Energy Mater. Sol. Cells* **2016**, *150*, 95−101.
(44) Triplett, M.; Yang, Y.; Léonard, F.; Talin, A. A.; Islam, M. S.; Yu, D. Long Minority Carrier Diffusion Lengths in Bridged Silicon Nanowires. *Nano Lett.* **2015**, *15*, 523−529.
(45) Léonard, F.; Talin, A. A. Electrical contacts to one- and two-dimensional nanomaterials. *Nat. Nanotechnol.* **2011**, *6*, 773−783.
(46) Talin, A. A.; Léonard, F.; Katzenmeyer, A. M.; Swartzentruber, B. S.; Picraux, S. T.; Toimil-Molares, M. E.; Cederberg, J. G.; Wang, X.; Hersee, S. D.; Rishinaramangalum, A. Transport characterization in nanowires using an electrical nanoprobe. *Semicond. Sci. Technol.* **2010**, *25*, No. 024015.
(47) Katzenmeyer, A. M.; Léonard, F.; Talin, A. A.; Wong, P.-S.; Huffaker, D. L. PooleFrenkel Effect and Phonon-Assisted Tunneling in GaAs Nanowires. *Nano Lett.* **2010**, *10*, 4935−4938.
(48) Talin, A. A.; Léonard, F.; Swartzentruber, B. S.; Wang, X.; Hersee, S. D. Unusually Strong Space-Charge-Limited Current in Thin Wires. *Phys. Rev. Lett.* **2008**, *101*, No. 076802.
(49) Murgatroyd, P. N. Theory of space-charge-limited current enhanced by Frenkel effect. *J. Phys. D: Appl. Phys.* **1970**, *3*, 151−156.
(50) Joshi, P. C.; Krupanidhi, S. B. Structural and electrical characteristics of $SrTiO_3$ thin films for dynamic random access memory applications. *J. Appl. Phys.* **1993**, *73*, 7627−7634.
(51) Neville, R. C.; Hoeneisen, B.; Mead, C. A. Permittivity of Strontium Titanate. *J. Appl. Phys.* **1972**, *43*, 2124−2131.
(52) Talin, A. A.; Wang, G. T.; Lai, E.; Anderson, R. J. Correlation of growth temperature, photoluminescence, and resistivity in GaN nanowires. *Appl. Phys. Lett.* **2008**, *92*, No. 093105.

https://doi.org/10.1021/acsnano.3c01448
ACS Nano 2023, 17, 9405−9414

(53) Smit, G. D. J.; Rogge, S.; Klapwijk, T. M. Enhanced tunneling across nanometer-scale metal−semiconductor interfaces. *Appl. Phys. Lett.* **2002**, *80*, 2568−2570.
(54) Kraya, R. A.; Kraya, L. Y. The role of contact size on the formation of Schottky barriers and ohmic contacts at nanoscale metal-semiconductor interfaces. *J. Appl. Phys.* **2012**, *111*, No. 064302.
(55) Ruffino, F.; Grimaldi, M. G.; Giannazzo, F.; Roccaforte, F.; Raineri, V. Size-dependent Schottky Barrier Height in self-assembled gold nanoparticles. *Appl. Phys. Lett.* **2006**, *89*, 243113.
(56) Sullivan, J. P.; Tung, R. T.; Pinto, M. R.; Graham, W. R. Electron transport of inhomogeneous Schottky barriers: A numerical study. *J. Appl. Phys.* **1991**, *70*, 7403−7424.
(57) Tung, R. T. Recent advances in Schottky barrier concepts. *Materials Science and Engineering: R: Reports* **2001**, *35*, 1−138.
(58) Kawasaki, S.; Akagi, K.; Nakatsuji, K.; Yamamoto, S.; Matsuda, I.; Harada, Y.; Yoshinobu, J.; Komori, F.; Takahashi, R.; Lippmaa, M.; Sakai, C.; Niwa, H.; Oshima, M.; Iwashina, K.; Kudo, A. Elucidation of Rh-Induced In-Gap States of Rh: $SrTiO_3$ Visible- Light-Driven Photocatalyst by Soft X-ray Spectroscopy and First-Principles Calculations. *J. Phys. Chem. C* **2012**, *116*, 24445−24448.
(59) Swaminathan, V.; Macrander, A. *Materials Aspects of GaAs and InP Based Structures*; Prentice-Hall: Englewood Cliffs, NJ, 1992; pt 286.
(60) Frederikse, H. P. R.; Thurber, W. R.; Hosler, W. R. Electronic Transport in Strontium Titanate. *Phys. Rev.* **1964**, *134*, A442−A445.
(61) Wunderlich, W.; Ohta, H.; Koumoto, K. Enhanced effective mass in doped $SrTiO_3$ and related perovskites. *Physica B: Condensed Matter* **2009**, *404*, 2202−2212.
(62) Kittel, C. *Introduction to Solid State Physics*, 8th ed.; Wiley: Hoboken, NJ, 2005; p 441.
(63) Crespillo, M. L.; Graham, J. T.; Agulló-López, F.; Zhang, Y.; Weber, W. J. The blue emission at 2.8 eV in strontium titanate: evidence for a radiative transition of selftrapped excitons from unbound states. *Materials Research Letters* **2019**, *7*, 298−303.
(64) Esposito, D. V.; Levin, I.; Moffat, T. P.; Talin, A. A. H2 evolution at Si-based metal−insulator−semiconductor photoelectrodes enhanced by inversion channel charge collection and H spillover. *Nature Mater.* **2013**, *12*, 562−568.

https://doi.org/10.1021/acsnano.3c01448
ACS Nano 2023, 17, 9405−9414